CRYSTAL GROWTH & DESIGN

Article

pubs.acs.org/crystal

A Family of Metal–Organic Frameworks with a New Chair-Conformation Resorcin[4]arene-Based Ligand: Selective Luminescent Sensing of Amine and Aldehyde Vapors, and Solvent-Mediated Structural Transformations

Hang Zhang,[†] Jin Yang,*[,†] Ying-Ying Liu,[†] Shuyan Song,*[,‡] and Jian-Fang Ma*[,†]

[†]Key Laboratory of Polyoxometalate Science, Department of Chemistry, Northeast Normal University, Changchun 130024, P. R. China

[‡]State Key Laboratory of Rare Earth Resource Utilization, Changchun Institute of Applied Chemistry, Chinese Academy of Sciences, Changchun 130022, P. R. China

Supporting Information

ABSTRACT: By utilizing a new chair-conformation resorcin[4]arene-based octacarboxylate ligand, four functional metal–organic frameworks (MOFs), namely, $[(CH_3)_2NH_2]_4[Cd_2(L)]\cdot 4H_2O$ (**1**), $[(CH_3)_2NH_2]_4[Zn_2(L)]\cdot 2DMF\cdot 6H_2O$ (**2**), $[(CH_3)_2NH_2]_4[Co_2(L)]\cdot 2DMF\cdot 4H_2O$ (**3**), and $[(CH_3)_2NH_2]_2[Co_3(L)(H_2O)_{12}]$ (**4**) (H_8L = 2,8,14,20-tetramethylphenyl-4,6,10,12,16,18,22,24-octa-carboxymethoxy-resorcin[4]arene and DMF = *N*,*N*-dimethylformamide), were solvothermally synthesized and structurally characterized. In **1**, each L^{8-} anion bridges eight Cd(II) atoms to give a three-dimensional (3D) (4,8)-connected $(4^6)(4^{12}.6^{10}.8^6)$ framework. In isostructural **2** and **3**, each L^{8-} anion links eight adjacent Zn(II) or Co(II) atoms to yield a 3D (4,8)-connected $(4^6)(4^{11}.6^{12}.8^5)$ net. In **4**, each L^{8-} anion only bridges four Co(II) atoms by using its four carboxylates each in a monodentate coordination mode to generate an infinite one-dimensional (1D) chain. Remarkably, the highly selective luminescent sensing of amine and aldehyde vapors was studied for **1** and **2** as fluorescent sensors. Importantly, a solvent-induced structural transformation from the 1D chain to the 3D porous framework between **3** and **4** was also investigated in detail.

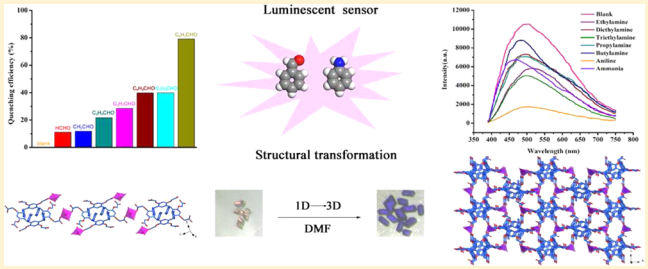

INTRODUCTION

Metal–organic frameworks (MOFs) have attracted a great deal of attention owing to their potential applications in catalysis, gas storage, chemical sensing, magnetic properties, etc.[1−15] In this regard, luminescent MOFs as fluorescent sensors have received intense interest for their huge superiority in unique photophysical properties.[16−18] The MOFs with variable structures and tunable fluorescence give them good selectivity.[19−21] Moreover, the molecular level interactions between the framework and the analytes could reduce detection limits, thereby showing high sensitivity.[22−24] Over the past several years, fluorescent MOFs have achieved great success in the trace detection of small organic molecules in liquid form.[25,26] Since the first report of the highly luminescent $[Zn_2(bpdc)_2(bpee)]$ (bpdc = 4,4′-biphenyldicarboxylate and bpee = 1,2-bipyridylethene) capable of detecting nitroaromatics in the vapor phase, studies employing the MOFs as luminescent sensors for vapor phase detections have been intensively pursued.[27] Very recently, a new two-dimensional (2D) mapping strategy has been developed for the effective detection of vaper analysts by using changes in fluorescence intensity and emission wavelength of the fluorescent MOF sensors.[28,29] Typical harmful vapors such as volatile aldehydes and amines are of great concern for the environment and food safety.[30,31] Therefore, fluorescent detecting of these volatile species has also become a significant topic.[32] However, only a few examples of fluorescent MOFs involving aldehyde or amine sensing in the vapor phase have been reported thus far.[33]

On the other hand, engineered MOFs involving transformations of their structures and properties by external stimuli, such as solvent, heat, guest removal, oxidation of metal centers, and light,[34−40] have received considerable current interest. Among various factors mentioned above, the effects of the solvents on the structural transformations which involve changes in structural dimensionality resulting from cleavage and regeneration of coordination bonds are particularly attractive.[41,42]

Usually, organic ligands have a very important role in the design and synthesis of functional MOFs.[43,44] In this context, the modified calixarenes with a large number of substituents became a new series of very versatile organic ligands.[45−50] In the case of resorcin[4]arenes, their body and/or rims could be modified, which greatly enriched the structural diversities of the functional

Received: February 9, 2016
Revised: March 28, 2016

DOI: 10.1021/acs.cgd.6b00213
Cryst. Growth Des. XXXX, XXX, XXX−XXX

Scheme 1. Synthesis of Resorcin[4]arene-Functionalized Octacarboxylic Acid H_8L

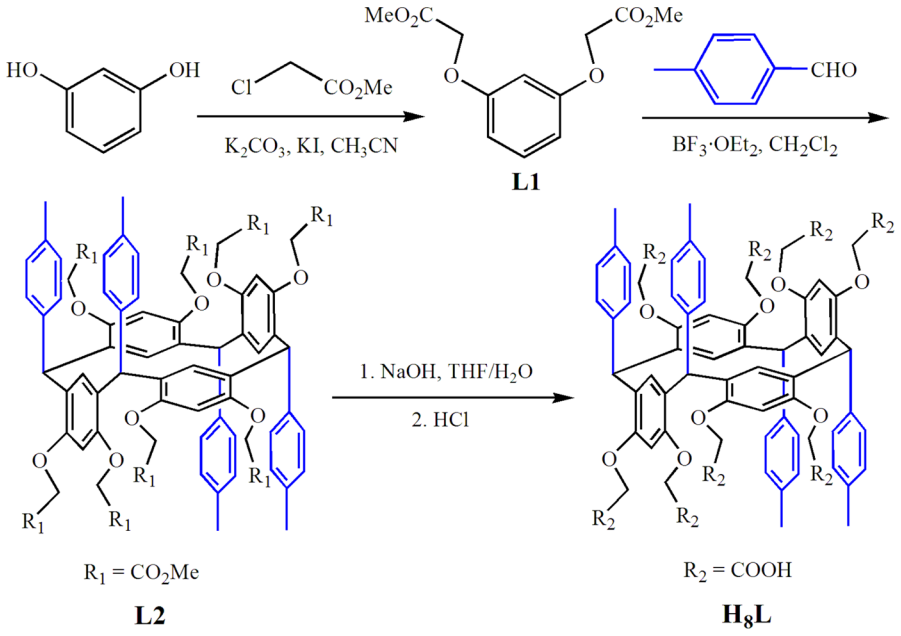

MOFs.[51,52] Several years ago, our group initiated a continuous investigation into the coordination chemistry of modified resorcin[4]arenes, and several series of resorcin[4]arenes-based MOFs, featuring fascinating motifs and properties, were reported.[51,53−58] Nevertheless, there is not a reported example that chair-conformation functionalized resorcin[4]arenes as organic linkers were employed for constructing functional MOFs.

On the basis of the above consideration, we synthesized a new resorcin[4]arene-functionalized octacarboxylate ligand, 2,8,14,20-tetra-methylphenyl-4,6,10,12,16,18,22,24-octa-carboxymethoxy-resorcin[4]arene (H_8L) (Scheme 1), in which two benzyl groups are at the upper edge of the resorcin[4]arene skeleton, and the remaining two are at the lower one, showing a chair conformation. By using the chair-conformation resorcin[4]arene-based octacarboxylate H_8L, four new MOFs, namely, $[(CH_3)_2NH_2]_4[Cd_2(L)]\cdot 4H_2O$ (**1**), $[(CH_3)_2NH_2]_4[Zn_2(L)]\cdot 2DMF\cdot 6H_2O$ (**2**), $[(CH_3)_2NH_2]_4[Co_2(L)]\cdot 2DMF\cdot 4H_2O$ (**3**), and $[(CH_3)_2NH_2]_2[Co_3(L)(H_2O)_{12}]$ (**4**) (DMF = *N*,*N*-dimethylformamide), have been synthesized and structurally characterized. Remarkably, the highly selective and sensitive luminescent probing of benzaldehyde and aniline vapors was explored for **1** and **2** as fluorescent sensors. More importantly, the solvent-induced structural transformation from the one-dimensional (1D) chain to the three-dimensional (3D) porous framework between **3** and **4** was also studied.

EXPERIMENTAL SECTION

Materials and Measurements. All chemical reagents were achieved from commercial sources. Powder X-ray diffraction (PXRD) patterns were determined on a Rigaku Dmax 2000 X-ray diffractometer. The FT-IR spectra were collected on a Mattson Alpha Centauri spectrometer. The UV−vis spectra were measured on a Cary 500 spectrophotometer. Elemental analysis data (C, H, and N) were collected on a PerkinElmer 240 elemental analyzer. The emission spectra are measured on a FLSP920 Edinburgh fluorescence spectrometer. Magnetic susceptibility data are collected on a SQUID magnetometer (Quantum Design, MPMS-5) with an applied field of 1000 Oe. Thermogravimetric data were determined on a PerkinElmer TG-7 analyzer.

Synthesis of l,3-Bis[(methoxycarbonyl)methoxy]benzene (L1). MeCN (300 mL) was added to a mixture of resorcinol (11.10 g, 100 mmol), anhydrous K_2CO_3 (34.5 g, 250 mmol), methyl chloroacetate (27.1 g, 250 mmol), and KI (0.5 g, 3 mmol). After heating at reflux for 48 h under nitrogen gas, the solvent was removed. A total of 200 mL of water was added to the residue, and the mixture was extracted by chloroform (3 × 200 mL). The organic phase was dried with anhydrous Na_2SO_4. After the chloroform was removed, the residue was recrystallized in methanol to afford L1 in a yield of 55%. Anal. Calcd for $C_{12}H_{14}O_6$ (M_r = 254.24): C, 56.69; H, 5.55. Found: C, 56.82; H, 5.41.

Synthesis of H_8L. A mixture of L1 (2.56 g, 10.0 mmol) and *p*-tolualdehyde (1.20 g, 10 mmol) in dichloromethane (30 mL) was stirred in an ice bath for 0.5 h with dropwise addition of $BF_3\cdot OEt_2$ (6 mL). Then the mixture was stirred at room temperature overnight. The solid was collected and washed by using CH_2Cl_2 to give L2 in a yield of 78%. Then sodium hydroxide (1.6 g, 40 mmol), tetrahydrofuran (150 mL), and water (150 mL) were added into the obtained L2. After heating at reflux for 8 h, the solvents were removed, and then 100 mL of water was added. pH value was adjusted to 1−2 by using HCl (1.0 mol·L^{-1}), and then the obtained solid was collected, washed with water, and dried in air to give H_8L in a yield of 60%. Anal. Calcd for $C_{72}H_{64}O_{24}$ (M_r = 1313.26): C, 65.85; H, 4.91. Found: C, 66.02; H, 4.65.

Synthesis of $[(CH_3)_2NH_2]_4[Cd_2(L)]\cdot 4H_2O$ (1). H_8L (0.027 g, 0.025 mmol) and $Cd(Ac)_2\cdot 2H_2O$ (0.012 g, 0.05 mmol) were dissolved in a mixture of DMF (6 mL) and H_2O (2 mL). Then the mixture was sealed in a Teflon reactor (15 mL) and heated at 110 °C for 3 days. Crystals of **1** were isolated in a 25% yield based on Cd(II) after cooling the Teflon reactor to room temperature. Anal. Calcd for $C_{80}H_{96}O_{28}N_4Cd_2$ (M_r = 1786.45): C, 53.70; H, 5.58; N, 3.01. Found: C, 53.82; H, 5.45; N, 3.14. IR data (KBr, cm^{-1}): 3421(w), 3048 (m), 3020(m), 2922(m), 2861(m), 2801(m), 2480(s), 1585(w), 1498(w), 1410(w), 1284(w), 1187(w), 1157(m), 1101(w), 1060(w), 1023(m), 926(s), 895(s), 857(s), 810(s), 720(s), 600(s), 698(s).

Synthesis of $[(CH_3)_2NH_2]_4[Zn_2(L)]\cdot 2DMF\cdot 6H_2O$ (2). A mixture of H_8L (0.027 g, 0.025 mmol), $Zn(Ac)_2\cdot 2H_2O$ (0.012 g, 0.05 mmol), DMF (4 mL), and H_2O (4 mL) was sealed in a Teflon reactor (15 mL) and heated at 120 °C for 3 days. Crystals of **2** were isolated in a 30% yield based on Zn(II) after cooling the Teflon reactor to room temperature. Anal. Calcd for $C_{86}H_{106}N_6O_{32}Zn_2$ (M_r = 1866.60): C, 55.39; H, 5.72; N, 4.56. Found: C, 55.26; H, 5.85; N, 4.44. IR data (KBr, cm^{-1}): 3440(m), 3254(m), 3154(m), 3050(m), 3021(w), 2913(m), 2857(m), 2784(m), 2523(s), 2427(s), 1667(w), 1626(w), 1586(w), 1500(w), 1471(m),

DOI: 10.1021/acs.cgd.6b00213
Cryst. Growth Des. XXXX, XXX, XXX−XXX

Table 1. Crystal Data and Structure Refinements for 1−4

	1	2	3	4
formula	$C_{80}H_{96}O_{28}N_4Cd_2$	$C_{86}H_{106}N_6O_{32}Zn_2$	$C_{86}H_{106}Co_2N_6O_{30}$	$C_{76}H_{86}Co_3O_{36}N_2$
M_r	1786.45	1866.60	1821.65	1780.28
space group	$C2/c$	$P2_1/n$	$P2_1/n$	$P\bar{1}$
a/Å	29.0460(9)	11.8040(5)	11.8380(8)	11.4780(8)
b/Å	21.4360(6)	24.8100(9)	24.7720(15)	12.2130(9)
c/Å	14.6820(5)	15.6720(7)	15.7730(8)	18.3460(13)
α/°	90	90	90	74.655(6)
β/°	93.618(3)	96.269(4)	96.834(5)	82.714(6)
γ/°	90	90	90	86.954(6)
V/Å^3	9123.2(5)	4562.2(3)	4592.6(5)	2459.5(3)
Z	8	4	4	1
D_c (g/cm^3)	1.301	1.359	1.317	1.202
GOF on F^2	0.999	1.019	1.015	1.175
$R1$[a] $[I > 2\sigma(I)]$	0.0555	0.0598	0.0818	0.1193
$wR2$[b] (all data)	0.1652	0.1625	0.2269	0.2863
R_{int}	0.0312	0.0436	0.0896	0.0620

[a] $R_1 = \Sigma||F_o| - |F_c||/\Sigma|F_o|$. [b] $wR_2 = \{\Sigma[w(F_o^2 - F_c^2)^2]/\Sigma w(F_o^2)^2]\}^{1/2}$.

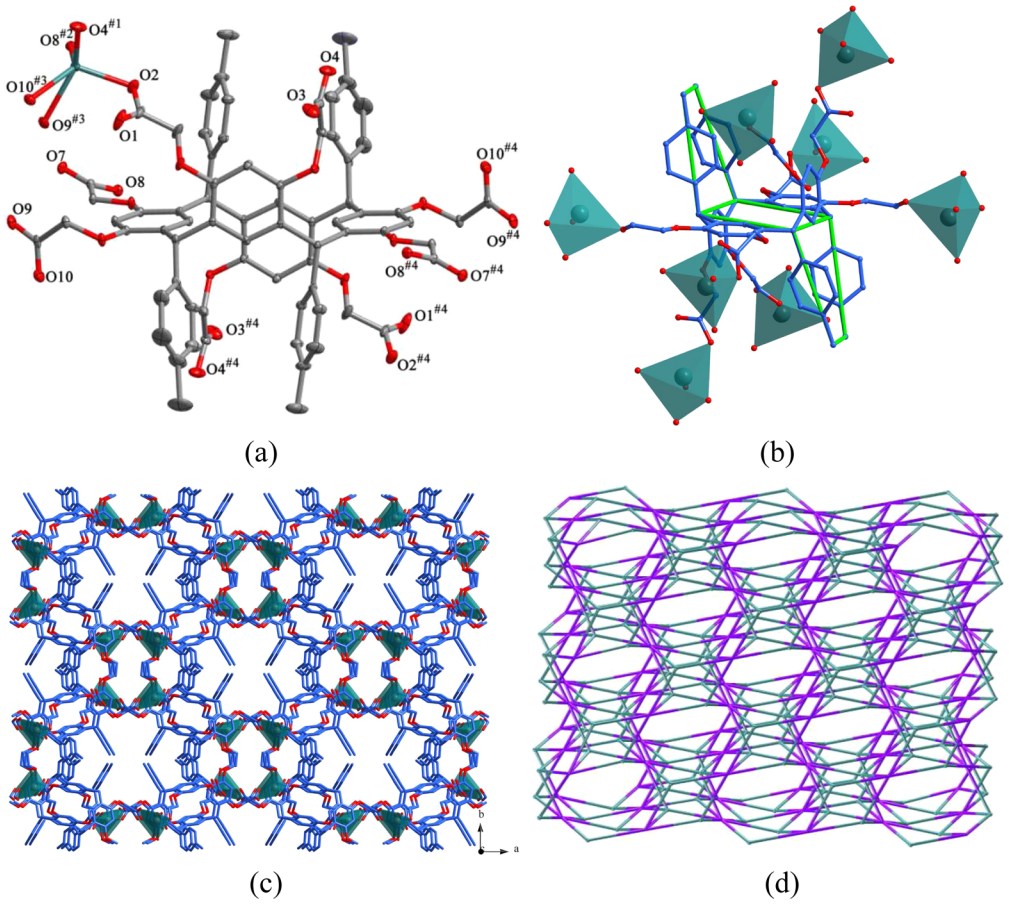

Figure 1. (a) View of the coordination environment of Cd(II) atom in **1**. (b) View of the coordination mode of L^{8-} anion. Symmetry codes: #1 $-x-1/2, -y+1/2, -z+1$; #2 $-x, y, -z+1/2$; #3 $-x-1/2, -y+1/2, -z$; #4 $x, -y+1, z+1/2$. (c) View of the 3D framework of **1**. (d) Schematic representation of the 3D (4,8)-connected net of **1**.

1420(w), 1342(s), 1314(w), 1280(w), 1257(w), 1189(w), 1156(m), 1100(w), 1062(w), 1025(m), 929(s), 899(s), 857(s), 809(s), 694(m), 664(s), 614(s), 594(s), 550(s), 509(s), 450(s), 412(s).

Synthesis of $[(CH_3)_2NH_2]_4[Co_2(L)]\cdot 2DMF\cdot 4H_2O$ (3). The synthesis of **3** is analogous to that of **1** except that $Co(Ac)_2\cdot 4H_2O$ (0.014 g, 0.05 mmol) was utilized instead of $Cd(Ac)_2\cdot 2H_2O$. Purple crystals of **3** were isolated in a 28% yield based on Co(II). Anal. Calcd for $C_{86}H_{106}Co_2N_6O_{30}$ (M_r = 1821.65): C, 56.64; H, 5.56; N, 4.97. Found: C, 56.78; H, 5.75; N, 4.72. IR data (KBr, cm^{-1}): 3401(m), 3048(m), 3020(m), 2924(w), 2860(m), 2485(s), 1716(m), 1651(w), 1609(w), 1584(w), 1497(w), 1286(w), 1187(w), 1156(m), 1102(m), 1062(w), 1024(m), 927(s), 896(s), 853(s), 812(s), 729(m), 693(m), 600(s), 502(s).

Synthesis of $[(CH_3)_2NH_2]_2[Co_3(L)(H_2O)_{12}]$ (4). The synthesis of **4** is analogous to that of **3** except that the ratio of DMF (4 mL) and H_2O (4 mL) was changed to 1:1. The pink crystals were achieved in a 18%

DOI: 10.1021/acs.cgd.6b00213
Cryst. Growth Des. XXXX, XXX, XXX−XXX

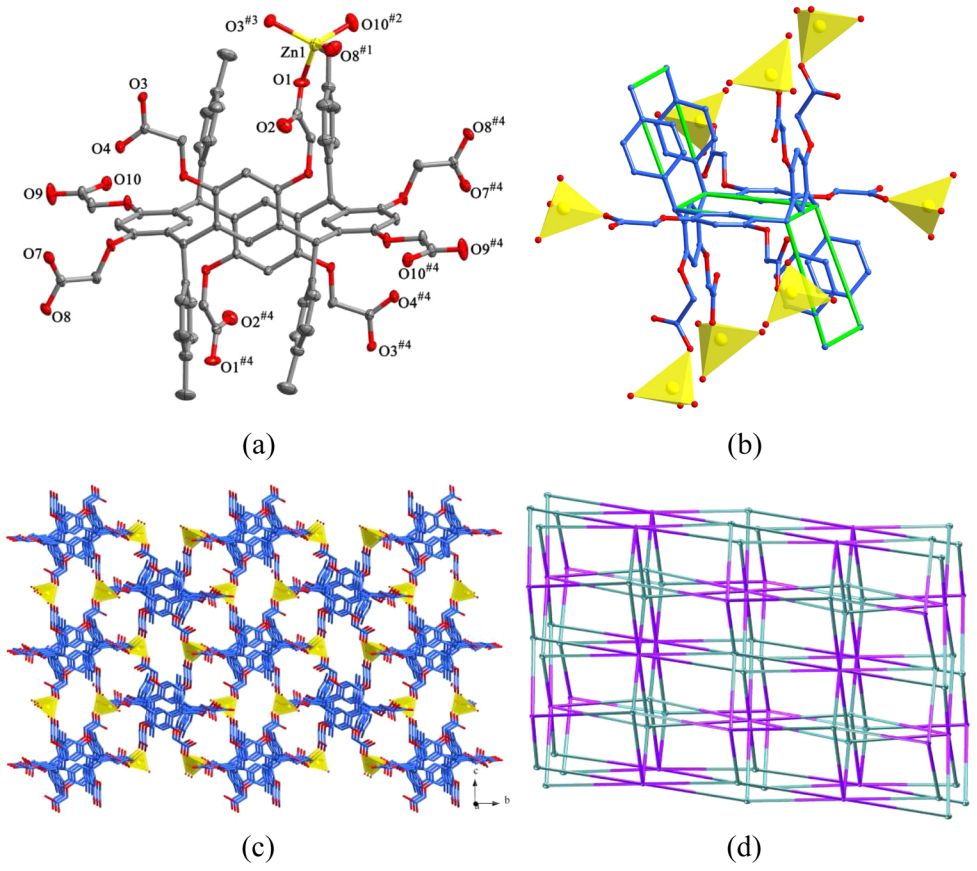

Figure 2. (a) Diagram showing the coordination environment of Zn(II) atom in **2**. Symmetry codes: #1 $-x-1/2, y-1/2, -z+3/2$; #2 $-x+1/2, y-1/2, -z+3/2$; #3 $-x, -y+1, -z+2$; #4 $-x, -y+1, -z+1$. (b) View of the coordination mode of L^{8-} anion. (c) View of the 3D framework of **2**. (d) Schematic representation of the (4,8)-connected $(4^6)(4^{11}.6^{12}.8^5)$ net of **2**.

yield based on Co(II). Anal. Calcd for $C_{76}H_{86}Co_3O_{36}N_2$ (M_r = 1780.28): C, 51.17; H, 4.91; N, 1.78. Found: C, 51.36; H, 4.79; N, 1.67. IR data (KBr, cm^{-1}): 3631(m), 3452(w), 3048(m), 3019(m) 2927(m), 2365(s), 2339(s), 1642(w), 1584(w), 1495 (w), 1427(w), 1329(m), 1290(m), 1232(m), 1188(w), 1155(w), 1096(w), 1058(w), 925(s), 874(s), 841(s), 811(m), 791(s), 772(s),739(m), 689(m), 642(s), 602(s), 550(s), 506(m).

Measurement for Luminescent Sensing of Volatile Aldehyde and Amine Vapors. The as-synthesized samples of **1** and **2** were immersed into anhydrous methanol for 3 days, and then the methanol solvent was refreshed three times during the exchange. After the removal of methanol by centrifuging, the wet sample was dried under a vacuum at 80 °C for 10 h to give the activated samples of **1** and **2**. Then, a small beaker (10 mL) with the activated samples (10 mg) was placed into a big sealed container (50 mL) with given solvent (20 mL) for 24 h (Figure S1). Subsequently, the small beaker was taken out from the container and quickly sealed, and the emission spectra were measured by using the solid samples. The initial emission spectrum of the solid sample was measured in a solid sample holder before exposure to various solvent vapors.

To test the response rate of **1** and **2** toward the benzaldehyde and aniline vapors, the time-dependent fluorescence quenching profile was measured. The activated samples of **2** (50 mg) were ground into powder, and then were further pressed into firm sheet samples. The firm sheet was stuck on a quartz slide through a double-side adhesive. The cuvette containing the sensor slide was adjusted to a suitable position (Figure S2). The solid state emission spectra of the firm sheet samples were determined as an original standard. Then, benzaldehyde or aniline solution (100 μL) was added into the cuvette by toppette pipettor. The cuvette was then sealed carefully by the cap. The emission spectra as well as the responses of the sensor slide versus time plots were measured in benzaldehyde or aniline vapors.

Crystal Structure Determinations. The intensity data of **1**–**4** were measured on a Oxford Diffraction Gemini R Ultra diffractometer with graphite-monochromated Mo–Kα radiation (λ = 0.71073 Å). Starting structural models were solved by direct method of SHELXS-97 and refined by full-matrix least-squares techniques on F^2 using the SHELXL-97 program within WINGX.[59−61] Non-hydrogen atoms were refined anisotropically. Hydrogen atoms of the water molecules were not located from the difference Fourier maps. During the refinements of **1** and **4**, the SQUEEZE functions in PLATON were applied to remove the contribution of reflection by disordered solvent molecules.[62] Further crystallographic details are listed in Table 1. Selected bond distances and angles are given in Tables S1–S4.

RESULTS AND DISCUSSION

Structure of $[(CH_3)_2NH_2]_4[Cd_2(L)]\cdot 4H_2O$ (1). The asymmetric unit of **1** consists of one Cd(II) cation, one-half-occupied L^{8-} anion, two $[H_2N(CH_3)_2]^+$ cations, and two lattice water molecules, as illustrated in Figure 1a. Each Cd(II) atom is surrounded by five carboxylate oxygen atoms from four different L^{8-} anions (Cd1–O2 = 2.234(5), Cd1–O4$^{\#1}$ = 2.190(4), Cd1–O8$^{\#2}$ = 2.352(3), Cd1–O9$^{\#3}$ = 2.449(3), Cd1–O10$^{\#3}$ = 2.261(3) Å) in a distorted trigonal bipyramid geometry. Remarkably, each L^{8-} anion exhibits a chair conformation and links eight Cd(II) cations by using its eight carboxylates (Figure 1b). In this manner, adjacent Cd(II) atoms are interconnected by L^{8-} anions to give an extended 3D framework, as illustrated in Figure 1c. It is noteworthy that the negative charges of the framework are balanced by $(CH_3)_2NH_2^+$ cations, which results from the decomposed DMF solvents (Figure S3a). After removal of the solvent molecules, the free volume calculated by PLATON

DOI: 10.1021/acs.cgd.6b00213
Cryst. Growth Des. XXXX, XXX, XXX–XXX

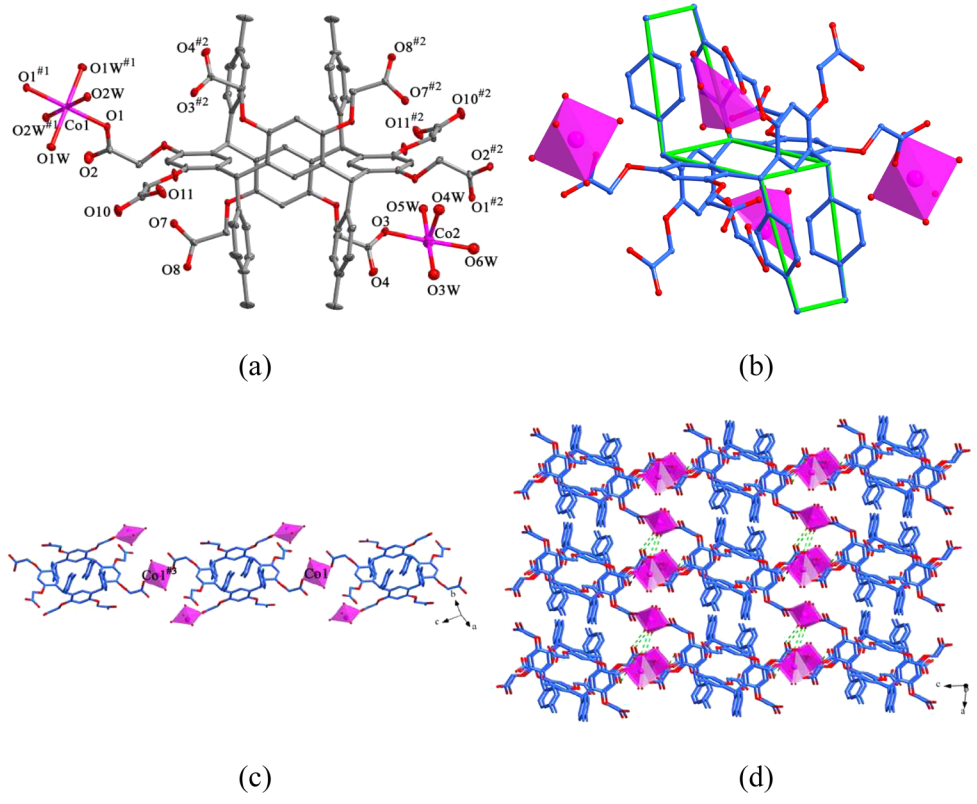

Figure 3. (a) Diagram showing the coordination environments of Co(II) atoms in **4**. Symmetry codes: $^{\#1}$ $-x + 1, -y, -z - 1$; $^{\#2}$ $-x, -y, -z$. (b) Coordination mode of the L^{8-} anion. (c) View of the 1D chain in **4**. (d) View of the 3D supramolecular architecture of **4**.

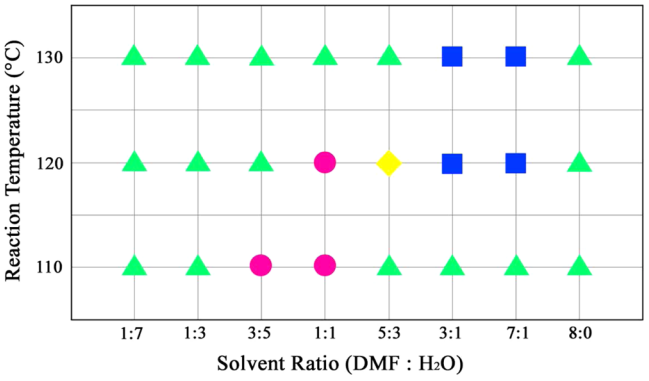

Figure 4. A diagram showing the parameters of solvent ratio and reaction temperature. Unknown phase (green triangles), powder phase of **3** (yellow circle), pure crystalline phase of **3** (blue square), pure crystalline phase of **4** (pink circle).

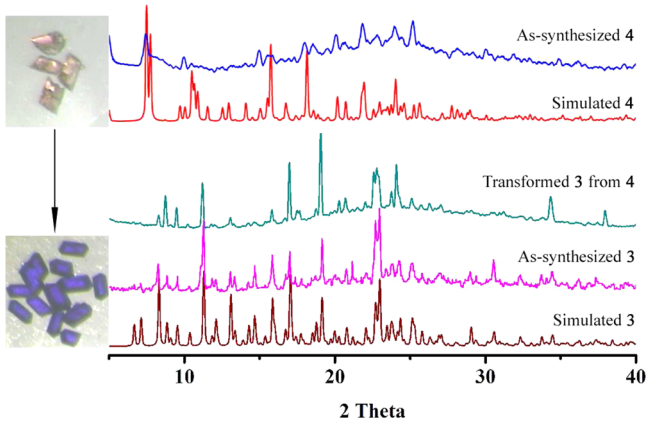

Figure 5. Photographs and PXRD patterns of as-synthesized **4** and after being handled by DMF.

analysis is ca. 38.1%.[62] Topologically, if both Cd(II) atom and L^{8-} anion can be classified as 4- and 8-connected nodes, respectively, the overall 3D framework of **1** can be described as a (4,8)-connected $(4^6)(4^{12}.6^{10}.8^6)$ net (Figure 1d).

Structures of $[(CH_3)_2NH_2]_4[Zn_2(L)]\cdot 2DMF\cdot 6H_2O$ (2) and $[(CH_3)_2NH_2]_4[Co_2(L)]\cdot 2DMF\cdot 4H_2O$ (3). Compounds **2** and **3** are isostructural (Figure S4) and crystallize in the same monoclinic space group $P2_1/n$. Hence, only the structure of **2** is described here. As illustrated in Figure 2a, the asymmetric unit of **2** is composed of one Zn(II) cation, one-half-occupied L^{8-} anion, two $[H_2N(CH_3)_2]^+$ cations, three lattice water molecules, and one lattice DMF molecule. Each Zn(II) atom is in a distorted tetrahedral sphere, coordinated by four carboxylate oxygen atoms from four different L^{8-} anions (Zn1−O1 = 1.942(2), Zn1−O3$^{\#3}$ = 1.967(2), Zn1−O8$^{\#1}$ = 1.925(2), Zn1−O10$^{\#2}$ = 1.939(2) Å). Each carboxylate of the L^{8-} anion displays a monodentate coordination mode (Figure 2b). In this manner, each L^{8-} anion bridges adjacent eight Zn(II) cations to yield a 3D framework (Figure 2c). Topologically, if both Zn(II) atom and L^{8-} anion are considered as 4- and 8-nodes, respectively, the overall structure of **2** can be simplified as a (4,8)-connected $(4^6)(4^{11}.6^{12}.8^5)$ net (Figure 2d). For **2** and **3**, the solvent-accessible volumes calculated by PLATON analysis are 36.8% and 36.3%, respectively, after removal of the solvent molecules.[62] Moreover, the void dimensions for **1** and **2** are ca. 4.0 and ca. 5.4 Å, respectively, as shown in Figure S5.

Structure of $[(CH_3)_2NH_2]_2[Co_3(L)(H_2O)_{12}]$ (4). As depicted in Figure 3a, the asymmetric unit of **4** contains one and a half

DOI: 10.1021/acs.cgd.6b00213
Cryst. Growth Des. XXXX, XXX, XXX−XXX

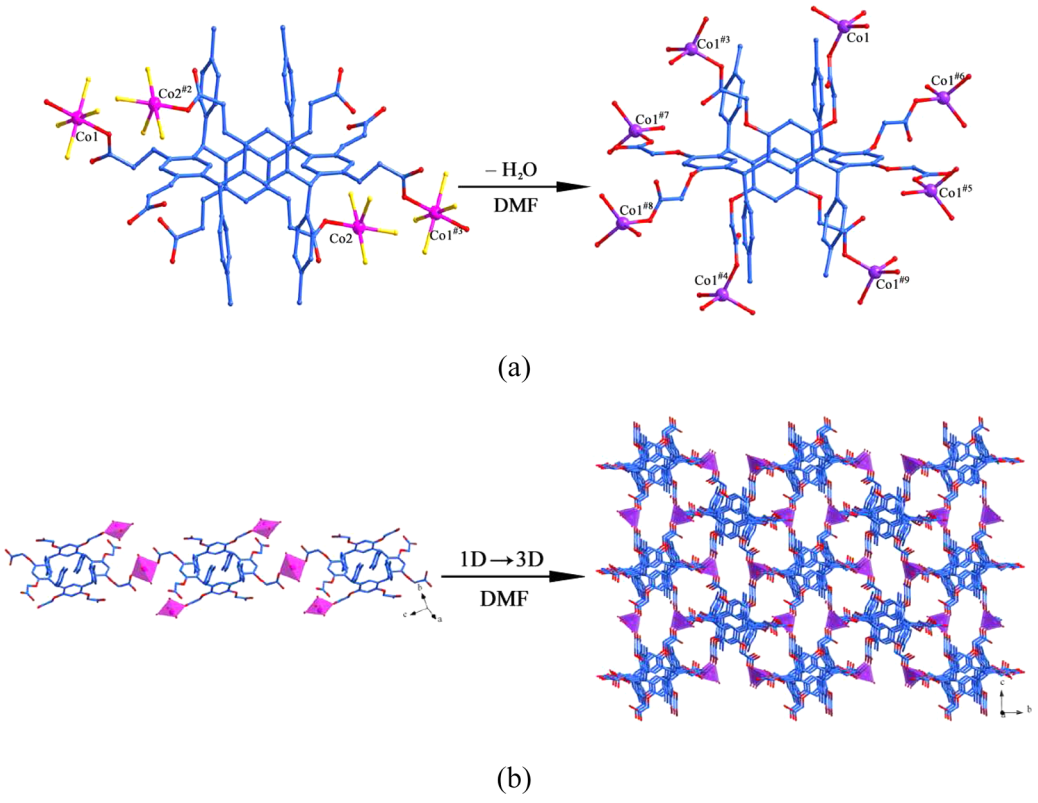

Figure 6. (a) Changes of coordination environments of Co(II) atoms and coordination modes of L^{8-} anions. The yellow ball and red ball represent water oxygen atom and carboxylate oxygen atom, respectively. (b) View of the solvent-induced structural transformation from **4** to **3**.

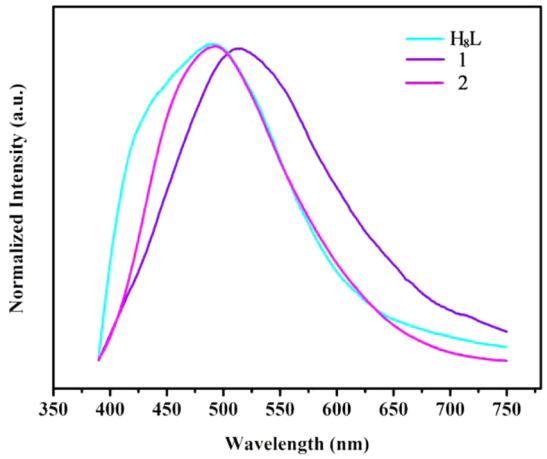

Figure 7. Emission spectra of H_8L, **1**, and **2** in solid state at room temperature.

Co(II) cations, one-half-occupied L^{8-} anion, and one $[H_2N(CH_3)_2]^+$ cation (Figure S3b). Notably, two Co(II) cations show different coordination modes. Co1, lying at an inversion center, is coordinated by two carboxylate oxygen atoms of two different L^{8-} anions (Co1–O1 = 2.077(4), Co1–$O1^{\#1}$ = 2.078(4) Å) and four water oxygen atoms (Co1–O1W = 2.095(4), Co1–O2W = 2.101(4), Co1–$O1W^{\#1}$ = 2.095(4), Co1–$O2W^{\#1}$ = 2.101(4) Å) in an octahedral environment. Co2 is coordinated by one carboxylate oxygen atom from one L^{8-} anion (Co2–O3 = 2.136(5) Å) and four water oxygen atoms (Co2–O3W = 2.068(13), Co2–O4W= 1.967(13), Co2–O6W = 2.046(15), Co2–O5W = 2.066(17) Å) in a distorted pyramidal coordination geometry (Figure 3a). Different from those in **1**–**3**, each L^{8-} anion in **4** only bridges four Co(II) atoms by using its four carboxylates each in a monodentate coordination mode (Figure 3b). In this fashion, Co1 and its symmetry-related species are bridged by L^{8-} anions to give an infinite 1D chain, as depicted in Figure 3c. Co2 and its symmetry-related ones are located on both sides of the chain. Noticeably, the short O···O contacts between water molecules and L^{8-} anions (O1W···O1 = 2.615 Å, O2W···O10 = 2.727 Å and O4W···O10 = 2.584 Å) suggest the existence of O–H···O hydrogen bonds, although the hydrogen atoms of the O1W, O2W, and O4W were not located from the difference Fourier maps. Further, adjacent 1D chains are linked by the O···O contacts into a 3D supramolecular architecture (Figure 3d).

Solvent-Induced Structural Transformation between 3 and 4. During the syntheses of Co(II)-based compounds **3** and **4**, we found that the solvent ratio and reaction temperature have crucial roles in the formation of their resulting frameworks. As a result, numerous parallel experiments were performed by varying the solvent ratios as well as the reaction temperatures. To give an overview of synthetic conditions of **3** and **4**, a diagram showing the parameters of solvent ratios and reaction temperatures is provided in Figure 4. When the solvent ratios (DMF/H_2O) are 1:7 and 1:3, no crystals of **3** and **4** are produced at all temperature ranges. By increasing the solvent ratio to 3:5 or 1:1, crystals of **3** could be obtained at 110 or 120 °C. When the solvent ratio reaches 5:3, a powder phase of **3** appears at 120 °C, which was confirmed by PXRD patterns (Figure S6). By further increasing the solvent ratio to 3:1 or 7:1, only crystals of **3** were formed at 120 °C or above temperature. The above results demonstrate that crystals of **3** can be easily produced from the components with a high solvent ratio between DMF and water at relatively

DOI: 10.1021/acs.cgd.6b00213
Cryst. Growth Des. XXXX, XXX, XXX–XXX

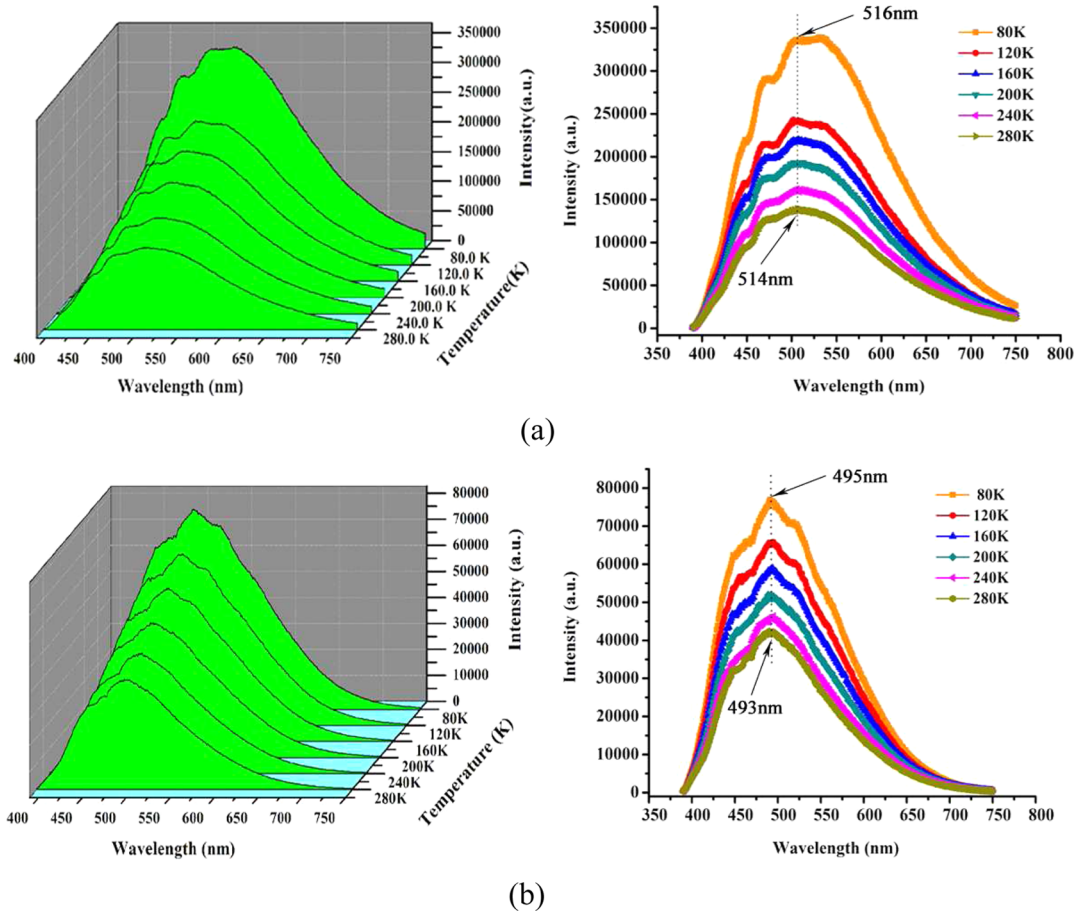

Figure 8. Luminescent intensities of **1** (a) and **2** (b) in the temperature range of 80−280 K.

high temperatures. When the solvent ratio (DMF/H_2O) and the reaction temperature were reduced, crystals of **4** were formed.

3 and **4** is assembled from the identical materials under similar conditions, which encouraged us to explore their possible structural conversion further. Fortunately, upon handling the as-synthesized **4** in DMF at 120 °C for 48 h, **4** undergoes a solvent-induced structural transformation to form **3**. As shown in Figure 5, the crystal colors changed from pale pink to purple. Both single crystal X-ray diffraction and PXRD patterns confirm that crystals of **4** have completely transformed into **3**. This transformation is proposed to probably be a solvent-induced structural transformation, which may involve the dissolution of **4** and recrystallization of **3** in DMF. Very recently, a striking single-crystal-to-single-crystal (SCSC) transformation associated with the dissolution and recrystallization process from the achiral $[Ni(NO_2\text{-ip})(bimb)(\mu\text{-}H_2O)]_n{\cdot}(H_2O)_n$ to chiral $[Ni_4(NO_2\text{-ip})_3(bimb)_2(OH)_2(H_2O)]_n{\cdot}(CH_3CH_2OH)_{0.5n}$ (NO_2-H_2ip = 5-nitroisophthalic acid and bimb = 1,4-bis(imidazol-1′-yl)butane) has been observed.[63] It should be mentioned that no single crystals of **3** were achieved when raw materials were treated in DMF at 120 °C. Thus, this solvent-induced structural transformation provides an alternative method for the crystal synthesis of **3**.

The solvent-induced structural transformation from **4** to **3** is involved in the cleavage and regeneration of Co−O bonds. As shown in Figure 6a, each Co(II) atom in **4** is surrounded by six oxygen atoms from four water molecules and two carboxylates, while the Co1 center in **3** is only coordinated by four carboxylate oxygen atoms. With the increasing ratio between DMF and water, the Co−O (water) bonds are gradually broken in **4**, and the new Co(II)−O (carboxylate) bonds are formed in **3**, leading to the 1D chain into the 3D framework (Figure 6b).

Luminescent Properties. MOFs containing d^{10} metals have attracted considerable attention because of their promising application as luminescent sensor materials.[64−66] The solid state emission spectra of free H_8L ligand, **1**, and **2** are measured at room temperature, as shown in Figure 7. Upon excitation at 323 nm, the free H_8L ligand displays an emission peak at 490 nm, which probably accounts for the $\pi^* \rightarrow \pi$ or $\pi^* \rightarrow n$ transitions.[67,68] Compounds **1** and **2** show emissions at 514 (λ_{ex} = 324 nm) and 493 nm (λ_{ex} = 324 nm), respectively, which are mainly based on the H_8L ligand because of their similar emission peaks.[69,70]

To explore the effect of measurement temperature on the luminescent intensities, the emission spectra of **1** and **2** were measured in the temperature range of 80−280 K (λ_{ex} = 324 nm). Notably, the luminescent intensities of **1** and **2** at 80 K are drastically enhanced compared to those at 280 K, as illustrated in Figure 8. As the temperatures increase, the emission bands of **1** and **2** are slightly blue-shifted. The above results can be attributed to the thermally active phononassisted tunneling between the excited states of low-energy site and the excited states of high-energy site.[71,72]

Luminescent Sensing of Aldehyde Vapors. Aldehydes, as important chemical raw materials and solvents, are very harmful to human health and environment as indoor pollutants.[73] Thereby, the development of a detection method for aldehydes is a significant topic in view of environmental and safety

DOI: 10.1021/acs.cgd.6b00213
Cryst. Growth Des. XXXX, XXX, XXX−XXX

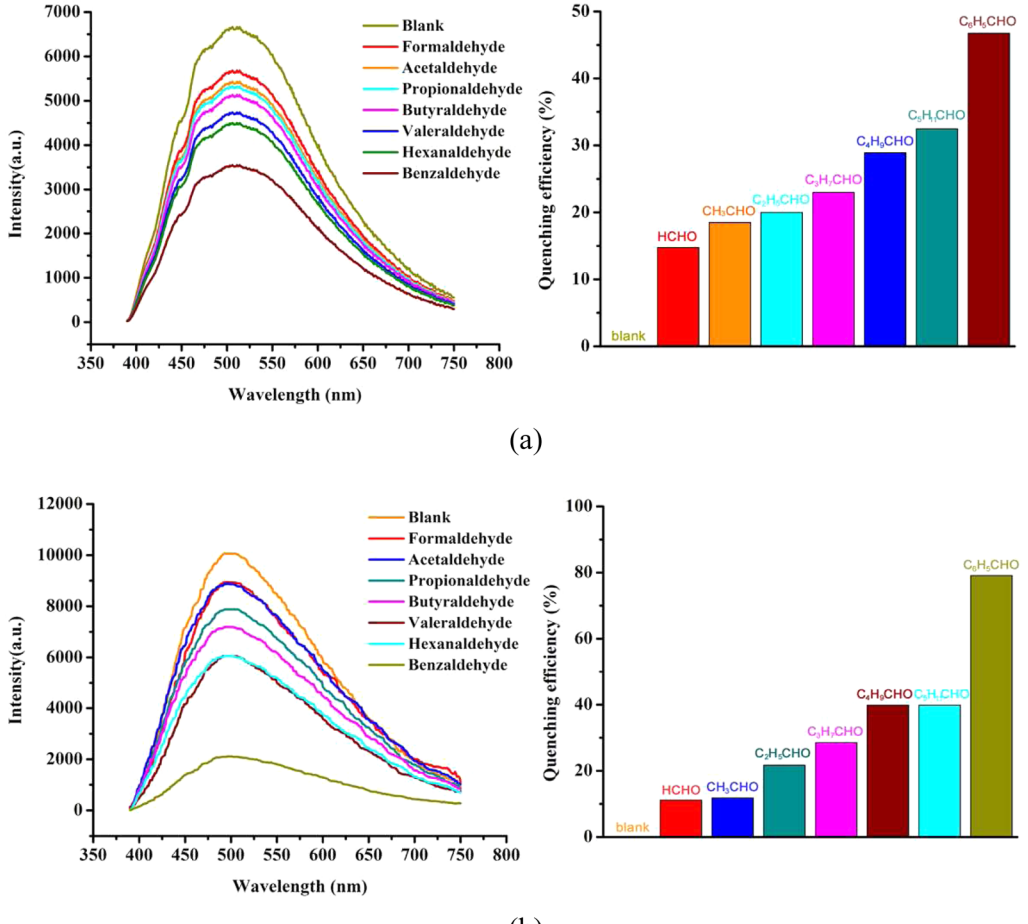

Figure 9. Luminescent intensity and quenching efficiency for the activated **1** (a) and **2** (b) in various aldehyde vapors.

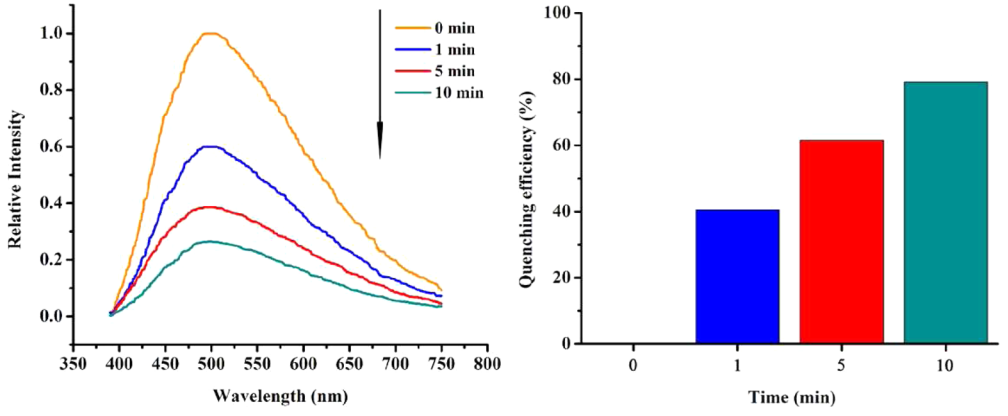

Figure 10. Luminescent intensity and quenching efficiency for the activated **2** upon exposure to benzaldehyde vapor at different time intervals.

considerations.[74] Among various types of analytical tools for the probing of aldehyde vapors, fluorescent sensors have been considered as a highly sensitive and selective detection method.[75] Notably, two recently reported lanthanide MOFs $[Ln(H_2DMPhIDC)_3(H_3DMPhIDC)]_n$ (Ln = Eu, Tb; $H_3DMPhIDC$ = 2-(3,4-dimethylphenyl)-1*H*-imidazole-4,5-dicarboxylic acid) show highly sensitive sensing of benzaldehyde-based derivatives.[73] In this study, the activated **1** and **2** were selected as luminescent sensors to probe organic aldehyde vapors, such as formaldehyde (HCHO), acetaldehyde (CH_3CHO), propionaldehyde (C_2H_5CHO), butyraldehyde (C_3H_7CHO), valeraldehyde (C_4H_9CHO), hexanaldehyde ($C_5H_{11}CHO$), and benzaldehyde (C_6H_5CHO). As depicted in Figure 9, the aldehyde vapors exhibit different degrees of luminescent quenching effects on the activated **1** and **2**. In other words, the luminescent intensities of the activated **1** and **2** are greatly dependent on aldehyde vapors. For the activated **1** and **2**, the benzaldehyde vapors show the most quenching effects with the quenching efficiency of 46.7% and 79.1%, respectively. Thus, the activated **1** and **2** are good candidates for the recognition of benzaldehyde vapors from other aldehydes. From the estimated electron numbers by the procedure SQUEEZE,[62] one benzaldehyde and two benzalde-

DOI: 10.1021/acs.cgd.6b00213
Cryst. Growth Des. XXXX, XXX, XXX−XXX

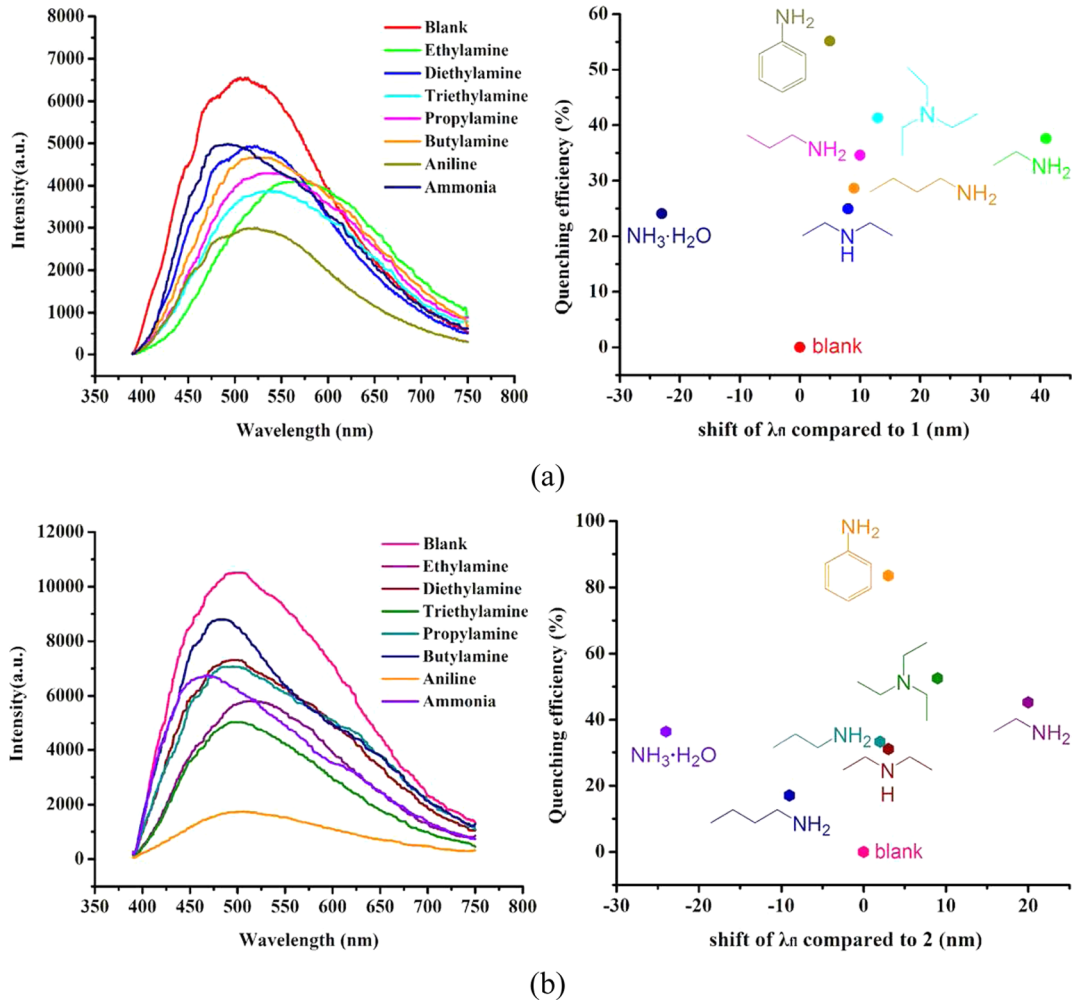

Figure 11. Luminescent intensity and relationship of quenching efficiency versus shift of λ_{fl} with respect to activated **1** (a) and **2** (b) in various amine vapors.

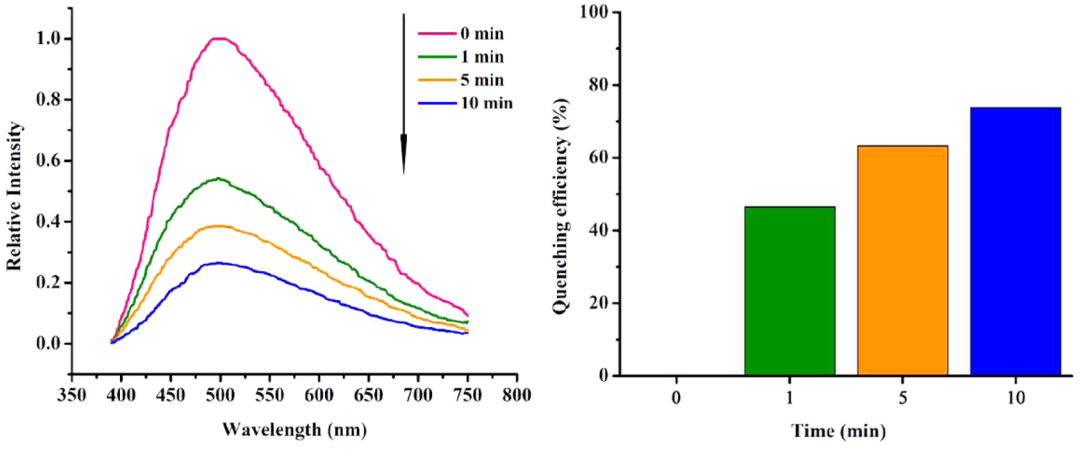

Figure 12. Luminescent intensity and quenching efficiency of the activated **2** upon exposure to the aniline vapor at different time intervals.

hyde molecules could be accommodated in the voids of **1** and **2**, respectively. Moreover, the activated samples in various aldehyde vapors show the same PXRD patterns (Figure S7), indicating that the activated **1** and **2** are stable in the luminescent sensing process.

For the sake of testing the luminescent responses of the activated **2** to the benzaldehyde vapor, the time-dependent fluorescent spectra upon exposure to benzaldehyde vapor were measured in different time intervals (Figure 10). Under benzaldehyde vapors, the luminescent intensity of the activated **2** gradually decreases with increasing time, and the quenching percentage reaches 73.8% within 10 min (Figure 10). The result indicates that the activated **2** is a potential solid-state fluorescent material for sensing of benzaldehyde vapor with a rapid response.

DOI: 10.1021/acs.cgd.6b00213
Cryst. Growth Des. XXXX, XXX, XXX−XXX

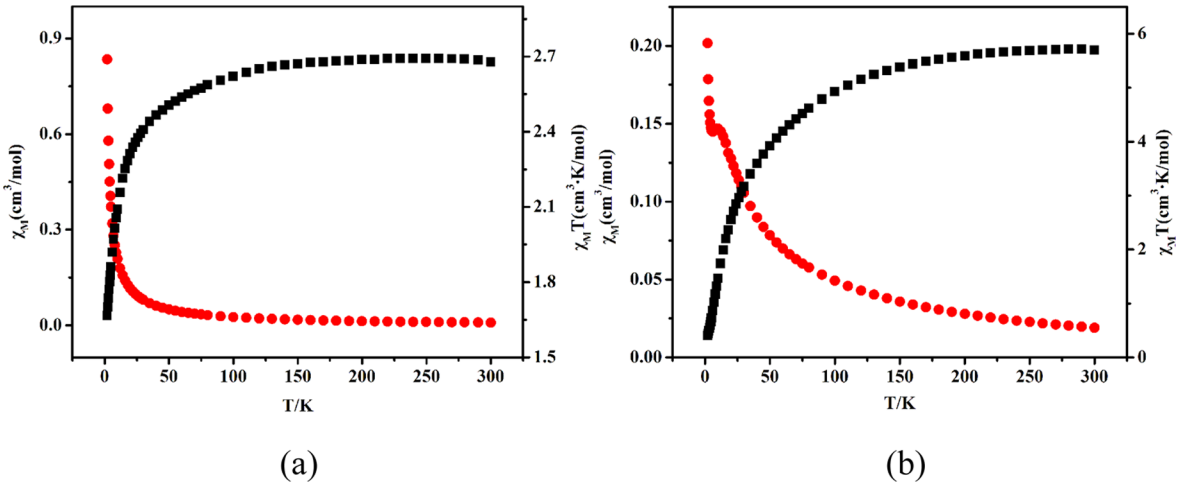

Figure 13. X_mT vs T curves for **3** (a) and **4** (b) in an applied field of 1000 Oe.

Luminescent Sensing of Amine Vapors. The detection of amines is critical in terms of the quality control of food and medical diagnosis, and has gained increasing attention.[76−79] Hence, the potential of activated **1** and **2** for the sensing of amine vapors, such as ethylamine ($C_2H_5NH_2$), propylamine ($C_3H_7NH_2$), butylamine ($C_4H_9NH_2$), diethylamine ($(C_2H_5)_2NH$), triethylamine ($(C_2H_5)_3N$), ammonia ($NH_3·H_2O$), and aniline ($C_6H_5NH_2$), was also explored. As shown in Figure 11, activated **1** and **2** exhibit an obvious decrease in the luminescent intensity under the amine vapors. The aniline vapor is the most quenching effective one for activated **1** and **2**. The most quenching efficiencies of aniline reach 55.1% and 85.2% for activated **1** and **2**, respectively, which is much higher than the second one of triethylamine (Figure 11). Moreover, noticeable shifts of the emission maxima (λ_{fl}) in the emission spectra were also observed. In contrast to the pristine emission peaks of the activated **1** (λ_{fl} = 514 nm) and **2** (λ_{fl} = 493 nm), apparent blue shifts of 23 and 24 nm were respectively observed for the activated **1** and **2** exposed to ammonia vapors. Nevertheless, obvious red shifts of 41 and 20 nm were respectively found for the activated **1** and **2** upon exposure to ethylamine vapors, as illustrated in Figure 11. The above observation indicates that the interactions between amines and ligands/MOFs may trigger peak shifts and responsive turn off fluorescence.[80,81] From the estimated electron numbers by the procedure SQUEEZE,[62] one aniline and two aniline molecules could be accommodated in the voids of **1** and **2**, respectively. Moreover, PXRD patterns of the activated samples in various amine vapors are nearly identical to the simulated one (Figure S8), suggesting that the structures of the activated **1** and **2** remained unchanged during the luminescent sensing process.

Moreover, the time-dependent fluorescent spectra for activated **2** were also studied under the aniline vapors. As illustrated in Figure 12, the luminescent intensities for activated **2** decreased drastically upon exposure to aniline vapors, and the quenching percentage reaches 79.3% within 10 min. Notably, after 24 h, the fluorescence quenching percentage of the aniline vapor is near 85.2%, suggesting that activated **2** is a potential fluorescent sensor for the aniline vapors.

To explore the fluorescent quenching process toward aldehyde and amine vapors, the UV−vis diffuse reflectance spectra of **1**, **2**, aldehydes, and amines were determined (Figure S9). The UV−vis absorption bands of both **1** and **2** are located in the range of 240−300 nm, which is probably ascribed to $\pi^* \rightarrow \pi$ or $\pi^* \rightarrow n$ transitions of the ligands.[82] Notably, the absorption bands of **1** and **2** are almost entirely overlapped by the wide absorption bands of benzaldehyde and aniline. Obviously, the overlap of the absorption bands causes a competition for excitation energy between the analysts (benzaldehyde and aniline) and MOFs, finally leading to a decrease or even quenching in luminescence intensities.[83] This luminescent process corresponds to the ones previously proposed by other groups.[84−87]

Magnetic Properties. Magnetic susceptibility data of **3** and **4** were collected at 2−300 K in an applied field of 1000 Oe (Figure 13). The χ_mT value of **3** is 2.76 cm^3 K·mol^{-1} at 300 K, which is slightly higher than the spin-only value for a high-spin Co(II) center (S = 3/2, 1.875 cm^3 K mol^{-1}).[88,89] Upon cooling, χ_mT value continuously decreases and reaches to 1.66 cm^3 K mol^{-1} at 2 K. The low temperature decrease of the susceptibility data is attributed to antiferromagnetic exchange interaction between the Co(II) centers and zero-field interactions.[90,91] The χ_mT value of **4** is 5.70 cm^3 K·mol^{-1} at 300 K, which is higher than 3.75 cm^3 K mol^{-1} expected for two Co(II) centers with an S = 3/2.[92] Upon cooling, the χ_mT value decreases monotonically to 0.40 cm^3 K mol^{-1} at 2 K, demonstrating the presence of antiferromagnetic interaction between Co(II) centers. The magnetic susceptibility data of **3** (above 2 K) and **4** (above 20 K) well obey the Curie−Weiss law with Curie and Weiss constants of C = 2.72 cm^3 K mol^{-1} and θ = −3.16 for **3**, and C = 6.37 cm^3 K mol^{-1} and θ = −29.82 for **4** (Figure S10). The negative Weiss constants also indicate antiferromagnetic interactions between the Co(II) centers in **3** and **4**.[93,94]

CONCLUSIONS

In summary, four new MOFs were constructed with a new chair-conformation resorcin[4]arene-based octacarboxylate ligand by a solvothermal method. They feature diverse motifs and dimensionalities from the 1D to 3D structures. The fluorescent sensing studies reveal that **1** and **2** are highly selective and sensitive fluorescent sensors for aniline and benzaldehyde vapors. More importantly, **3** and **4** demonstrate a remarkable solvent-mediated structural transformation from a 1D chain to a 3D porous framework.

ASSOCIATED CONTENT

Supporting Information

The Supporting Information is available free of charge on the ACS Publications website at DOI: 10.1021/acs.cgd.6b00213.

DOI: 10.1021/acs.cgd.6b00213
Cryst. Growth Des. XXXX, XXX, XXX−XXX

Diagram of gas sensing equipment, TG curves of **1** and **4**, coordination environment of Co(II) atom in **3**, molecular structures of aniline and benzaldehyde, channel diameters of **1** and **2**, PXRD patterns of experimental ones from different solvent ratios, PXRD patterns of the activated **1** and **2** after exposed to different aldehyde and amine vapors, UV absorption spectra of **1**, **2**, aldehydes and amines, temperature dependence of χ_m^{-1} at 1000 Oe for **3** and **4**, FTIR spectra of **1**−**4**, PXRD patterns of **1**−**4**, emission spectrum of **3** in solid state and selected bond lengths and angles (PDF)

Accession Codes

CCDC 1451892−1451895 contains the supplementary crystallographic data for this paper. These data can be obtained free of charge via www.ccdc.cam.ac.uk/data_request/cif, or by emailing data_request@ccdc.cam.ac.uk, or by contacting The Cambridge Crystallographic Data Centre, 12 Union Road, Cambridge CB2 1EZ, UK; fax: +44 1223 336033.

AUTHOR INFORMATION

Corresponding Authors

*E-mail: yangj808@nenu.edu.cn (J.Y.).
*E-mail: songsy@ciac.ac.cn (S.-Y.S.).
*E-mail: majf247@yahoo.com. Fax: +86-431-85098620 (J.-F.M.).

Notes

The authors declare no competing financial interest.

ACKNOWLEDGMENTS

This work was supported by the National Natural Science Foundation of China (Grant No. 21277022, 21371030, 21301026 and 21471029).

REFERENCES

(1) Zhou, H. C.; Kitagawa, S. *Chem. Soc. Rev.* **2014**, *43*, 5415−5418.
(2) Sawano, T.; Thacker, N. C.; Lin, Z.; McIsaac, A. R.; Lin, W. B. *J. Am. Chem. Soc.* **2015**, *137*, 12241−12248.
(3) Zhang, Y.-B.; Furukawa, H.; Ko, N.; Nie, W.; Park, H. J.; Okajima, S.; Cordova, K. E.; Deng, H.; Kim, J.; Yaghi, O. M. *J. Am. Chem. Soc.* **2015**, *137*, 2641−2650.
(4) Madrahimov, S. T.; Gallagher, J. R.; Zhang, G.; Meinhart, Z.; Garibay, S. J.; Delferro, M.; Miller, J. T.; Farha, O. K.; Hupp, J. T.; Nguyen, S. T. *ACS Catal.* **2015**, *5*, 6713−6718.
(5) Khaletskaya, K.; Pougin, A.; Medishetty, R.; Rösler, C.; Wiktor, C.; Strunk, J.; Fischer, R. A. *Chem. Mater.* **2015**, *27*, 7248−7257.
(6) Millange, F.; Guillou, N.; Medina, M. E.; Férey, G.; Carlin-Sinclair, A.; Golden, K. M.; Walton, R. I. *Chem. Mater.* **2010**, *22*, 4237−4245.
(7) He, C.-T.; Jiang, L.; Ye, Z.-M.; Krishna, R.; Zhong, Z.-S.; Liao, P.-Q.; Xu, J.; Ouyang, G.; Zhang, J.-P.; Chen, X.-M. *J. Am. Chem. Soc.* **2015**, *137*, 7217−7223.
(8) Kreno, L. E.; Leong, K.; Farha, O. K.; Allendorf, M.; Van Duyne, R. P.; Hupp, J. T. *Chem. Rev.* **2012**, *112*, 1105−1125.
(9) Hu, Z.; Deibert, B. J.; Li, J. *Chem. Soc. Rev.* **2014**, *43*, 5815−5840.
(10) Aulakh, D.; Pyser, J. B.; Zhang, X.; Yakovenko, A. A.; Dunbar, K. R.; Wriedt, M. *J. Am. Chem. Soc.* **2015**, *137*, 9254−9257.
(11) Meihaus, K. R.; Fieser, M. E.; Corbey, J. F.; Evans, W. J.; Long, J. R. *J. Am. Chem. Soc.* **2015**, *137*, 9855−9860.
(12) Maza, W. A.; Padilla, R.; Morris, A. J. *J. Am. Chem. Soc.* **2015**, *137*, 8161−8168.
(13) Taylor, J. M.; Komatsu, T.; Dekura, S.; Otsubo, K.; Takata, M.; Kitagawa, H. *J. Am. Chem. Soc.* **2015**, *137*, 11498−11506.
(14) Dong, J.; Cui, P.; Shi, P.-F.; Cheng, P.; Zhao, B. *J. Am. Chem. Soc.* **2015**, *137*, 15988−15991.
(15) Wu, H.; Yang, J.; Su, Z.-M.; Batten, S. R.; Ma, J.-F. *J. Am. Chem. Soc.* **2011**, *133*, 11406−11409.
(16) Wei, Z.; Gu, Z.-Y.; Arvapally, R. K.; Chen, Y.-P.; McDougald, R. N.; Ivy, J. F.; Yakovenko, A. A.; Feng, D.; Omary, M. A.; Zhou, H.-C. *J. Am. Chem. Soc.* **2014**, *136*, 8269−8276.
(17) Li, H.-Y.; Wei, Y.-L.; Dong, X.-Y.; Zang, S.-Q.; Mak, T. C. W. *Chem. Mater.* **2015**, *27*, 1327−1331.
(18) Demel, J.; Kubát, P.; Millange, F.; Marrot, J.; Císařová, I.; Lang, K. *Inorg. Chem.* **2013**, *52*, 2779−2786.
(19) Wei, N.; Zhang, M.-Y.; Zhang, X.-N.; Li, G.-M.; Zhang, X.-D.; Han, Z.-B. *Cryst. Growth Des.* **2014**, *14*, 3002−3009.
(20) Shustova, N. B.; Cozzolino, A. F.; Reineke, S.; Baldo, M.; Dinca, M. *J. Am. Chem. Soc.* **2013**, *135*, 13326−13329.
(21) Shi, P.-F.; Hu, H.-C.; Zhang, Z.-Y.; Xiong, G.; Zhao, B. *Chem. Commun.* **2015**, *51*, 3985−3988.
(22) Lee, J. H.; Jaworski, J.; Jung, J. H. *Nanoscale* **2013**, *5*, 8533−8540.
(23) Tian, D.; Li, Y.; Chen, R.-Y.; Chang, Z.; Wang, G.-Y.; Bu, X.-H. *J. Mater. Chem. A* **2014**, *2*, 1465−1470.
(24) He, Y.-C.; Zhang, H.-M.; Liu, Y.-Y.; Zhai, Q.-Y.; Shen, Q.-T.; Song, S. Y.; Ma, J.-F. *Cryst. Growth Des.* **2014**, *14*, 3174−3178.
(25) Liu, X.-G.; Wang, H.; Chen, B.; Zou, Y.; Gu, Z.-G.; Zhao, Z.; Shen, L. *Chem. Commun.* **2015**, *51*, 1677−1680.
(26) Mallick, A.; Garai, B.; Addicoat, M. A.; Petkov, P.; Heine, T.; Banerjee, R. *Chem. Sci.* **2015**, *6*, 1420−1425.
(27) Lan, A. J.; Li, K. H.; Wu, H. H.; Olson, D. H.; Emge, T. J.; Ki, W.; Hong, M. C.; Li, J. *Angew. Chem., Int. Ed.* **2009**, *48*, 2334−2338.
(28) Hu, Z. C.; Tan, K.; Lustig, W. P.; Wang, H.; Zhao, Y. G.; Zheng, C.; Banerjee, D.; Emge, T. J.; Chabal, Y. J.; Li, J. *Chem. Sci.* **2014**, *5*, 4873−4877.
(29) Hu, Z. C.; Pramanik, S.; Tan, K.; Zheng, C.; Liu, W.; Zhang, X.; Chabal, Y. J.; Li, J. *Cryst. Growth Des.* **2013**, *13*, 4204−4207.
(30) Zhang, H.; Chen, D.; Ma, H.; Cheng, P. *Chem. - Eur. J.* **2015**, *21*, 15854−15859.
(31) Pablos, J. L.; Vallejos, S.; Muñoz, A.; Rojo, M. J.; Serna, F.; García, F. C.; García, J. M. *Chem. - Eur. J.* **2015**, *21*, 8733−8736.
(32) Rochat, S.; Swager, T. M. *Angew. Chem., Int. Ed.* **2014**, *53*, 9792−9796.
(33) Yi, F.-Y.; Wang, Y.; Li, J.-P.; Wu, D.; Lan, Y.-Q.; Sun, Z.-M. *Mater. Horiz.* **2015**, *2*, 245−251.
(34) Ge, J.-Y.; Wang, J.-C.; Cheng, J.-Y.; Wang, P.; Ma, J.-P.; Liu, Q.-K.; Dong, Y.-B. *Chem. Commun.* **2014**, *50*, 4434−4437.
(35) Guo, Y.; Yang, X.-L.; Wei, R.-J.; Zheng, L.-S.; Tao, J. *Inorg. Chem.* **2015**, *54*, 7670−7672.
(36) Wang, Y.; Wang, X.-G.; Yuan, B.; Shao, C.-Y.; Chen, Y.-Y.; Zhou, B.-B.; Li, M.-S.; An, X.-M.; Cheng, P.; Zhao, X.-J. *Inorg. Chem.* **2015**, *54*, 4456−4465.
(37) Wang, C.; Li, L.; Bell, J. G.; Lv, X.; Tang, S.; Zhao, X.; Thomas, K. M. *Chem. Mater.* **2015**, *27*, 1502−1516.
(38) Liu, J.; Tan, Y.-X.; Zhang, J. *Cryst. Growth Des.* **2012**, *12*, 5164−5168.
(39) Chatterjee, P. B.; Audhya, A.; Bhattacharya, S.; Abtab, S. M. T.; Bhattacharya, K.; Chaudhury, M. *J. Am. Chem. Soc.* **2010**, *132*, 15842−15845.
(40) Chen, D.-M.; Shi, W.; Cheng, P. *Chem. Commun.* **2015**, *51*, 370−372.
(41) Bhattacharya, S.; Bhattacharyya, A. J.; Natarajan, S. *Inorg. Chem.* **2015**, *54*, 1254−1271.
(42) Shen, P.; He, W.-W.; Du, D.-Y.; Jiang, H.-L.; Li, S.-L.; Lang, Z.-L.; Su, Z.-M.; Fu, Q.; Lan, Y.-Q. *Chem. Sci.* **2014**, *5*, 1368−1374.
(43) Zhang, Q.; Su, J.; Feng, D.; Wei, Z.; Zou, X.; Zhou, H.-C. *J. Am. Chem. Soc.* **2015**, *137*, 10064−10067.
(44) Lin, Z.-J.; Lü, J.; Hong, M. C.; Cao, R. *Chem. Soc. Rev.* **2014**, *43*, 5867−5895.
(45) Chen, L.; Chen, Q.; Wu, M.; Jiang, F.; Hong, M. C. *Acc. Chem. Res.* **2015**, *48*, 201−210.
(46) Bi, Y.; Du, S.; Liao, W. P. *Coord. Chem. Rev.* **2014**, *276*, 61−72.
(47) Shi, Q.; Luo, W.-Z.; Li, B.; Xie, Y.-P.; Zhang, T. *Cryst. Growth Des.* **2016**, *16*, 493−498.
(48) Su, K.; Jiang, F.; Qian, J.; Chen, L.; Pang, J.; Bawaked, S. M.; Mokhtar, M.; Al-Thabaiti, S. A.; Hong, M. C. *Inorg. Chem.* **2015**, *54*, 3183−3188.

DOI: 10.1021/acs.cgd.6b00213
Cryst. Growth Des. XXXX, XXX, XXX−XXX

(49) Lee, J. H.; Park, J.; Park, J.-W.; Ahn, H.-J.; Jaworski, J.; Jung, J. H. *Nat. Commun.* **2015**, *6*, 6650−6658.
(50) Su, K.; Jiang, F.; Qian, J.; Gai, Y.; Wu, M.; Bawaked, S. M.; Mokhtar, M.; Al-Thabaiti, S. A.; Hong, M. C. *Cryst. Growth Des.* **2014**, *14*, 3116−3123.
(51) Lv, L.-L.; Yang, J.; Zhang, H.-M.; Liu, Y.-Y.; Ma, J.-F. *Inorg. Chem.* **2015**, *54*, 1744−1755.
(52) Sémeril, D.; Matt, D. *Coord. Chem. Rev.* **2014**, *279*, 58−95.
(53) Zhang, S.-T.; Yang, J.; Wu, H.; Liu, Y.-Y.; Ma, J.-F. *Chem. - Eur. J.* **2015**, *21*, 15806−15819.
(54) Hu, Y.-J.; Yang, J.; Liu, Y.-Y.; Song, S. Y.; Ma, J.-F. *Cryst. Growth Des.* **2015**, *15*, 3822−3831.
(55) Dong, Y.-B.; Shi, H.-Y.; Yang, J.; Liu, Y.-Y.; Ma, J.-F. *Cryst. Growth Des.* **2015**, *15*, 1546−1551.
(56) Li, X.-T.; Li, J.; Li, M.; Liu, Y.-Y.; Song, S.-Y.; Ma, J.-F. *CrystEngComm* **2014**, *16*, 9520−9527.
(57) Zhang, H.; Jiang, W.; Yang, J.; Liu, Y.-Y.; Song, S. Y.; Ma, J.-F. *CrystEngComm* **2014**, *16*, 9939−9946.
(58) Jiang, W.; Zhang, H.; Yang, J.; Liu, Y.-Y.; Liu, H.-Y.; Ma, J.-F. *CrystEngComm* **2014**, *16*, 9638−9644.
(59) Sheldrick, G. M. *SHELXS-97, Programs for X-ray Crystal Structure Solution*; University of Göttingen: Göttingen, Germany, 1997.
(60) Sheldrick, G. M. *SHELXL-97, Programs for X-ray Crystal Structure Refinement*; University of Göttingen: Göttingen, Germany, 1997.
(61) Farrugia, L. J. *WINGX, A Windows Program for Crystal Structure Analysis*; University of Glasgow, Glasgow, UK, 1988.
(62) Spek, A. L. *J. Appl. Crystallogr.* **2003**, *36*, 7−13.
(63) Li, X.; Yu, Z.; Li, X.; Guo, X. *Chem. - Eur. J.* **2015**, *21*, 16593−16600.
(64) Xie, Z. G.; Ma, L. Q.; deKrafft, K. E.; Jin, A.; Lin, W. B. *J. Am. Chem. Soc.* **2010**, *132*, 922−923.
(65) Nagarkar, S. S.; Joarder, B.; Chaudhari, A. K.; Mukherjee, S.; Ghosh, S. K. *Angew. Chem., Int. Ed.* **2013**, *52*, 2881−2885.
(66) Rocha, J.; Carlos, L. D.; Paz, F. A. A.; Ananias, D. *Chem. Soc. Rev.* **2011**, *40*, 926−940.
(67) Zhang, Z.; Ma, J.-F.; Liu, Y.-Y.; Kan, W. Q.; Yang, J. *Cryst. Growth Des.* **2013**, *13*, 4338−4348.
(68) Thirumurugan, A.; Natarajan, S. *J. Chem. Soc., Dalton Trans.* **2004**, 2923−2928.
(69) Sahu, J.; Ahmad, M.; Bharadwaj, P. K. *Cryst. Growth Des.* **2013**, *13*, 2618−2627.
(70) Xu, B.; Xie, J.; Hu, H.-M.; Yang, X.-L.; Dong, F.-X.; Yang, M.-L.; Xue, G.-L. *Cryst. Growth Des.* **2014**, *14*, 1629−1641.
(71) Li, B.; Huang, R.-W.; Qin, J.-H.; Zang, S.-Q.; Gao, G.-G.; Hou, H.-W.; Mak, T. C. W. *Chem. - Eur. J.* **2014**, *20*, 12416−12420.
(72) Wang, X. D.; Wolfbeis, O. S.; Meier, R. J. *Chem. Soc. Rev.* **2013**, *42*, 7834−7869.
(73) Shi, B.; Zhong, Y.; Guo, L.; Li, G. *Dalton Trans.* **2015**, *44*, 4362−4369.
(74) Xing, Y. L.; Wang, S.; Mao, X. Z.; Zhao, X. B.; Wei, D. Z. *J. Fluoresc.* **2011**, *21*, 587−594.
(75) Zhao, H.; Li, X.; Li, W.; Wang, P.; Chen, S.; Quan, X. *RSC Adv.* **2014**, *4*, 36444−36450.
(76) Shen, X.; Yan, B. *J. Mater. Chem. C* **2015**, *3*, 7038−7044.
(77) Oliveri, I. P.; Malandrino, G.; Di Bella, S. *Inorg. Chem.* **2014**, *53*, 9771−9777.
(78) Rampfl, M.; Mair, S.; Mayer, F.; Sedlbauer, K.; Breuer, K.; Niessner, R. *Environ. Sci. Technol.* **2008**, *42*, 5217−5222.
(79) Lee, M. H.; Yoon, B.; Kim, J. S.; Sessler, J. L. *Chem. Sci.* **2013**, *4*, 4121−4126.
(80) He, H.; Song, Y.; Sun, F.; Bian, Z.; Gao, L.; Zhu, G.-S. *J. Mater. Chem. A* **2015**, *3*, 16598−16603.
(81) Zhang, M.; Feng, G.; Song, Z.; Zhou, Y.-P.; Chao, H.-Y.; Yuan, D.; Tan, T. T. Y.; Guo, Z.; Hu, Z.; Tang, B. Z.; Liu, B.; Zhao, D. *J. Am. Chem. Soc.* **2014**, *136*, 7241−7244.
(82) Guo, J.; Ma, J.-F.; Liu, B.; Kan, W. Q.; Yang, J. *Cryst. Growth Des.* **2011**, *11*, 3609−3621.
(83) Chen, J.; Yi, F.-Y.; Yu, H.; Jiao, S.; Pang, G.; Sun, Z.-M. *Chem. Commun.* **2014**, *50*, 10506−10509.
(84) Chen, B.; Yang, Y.; Zapata, F.; Lin, G.; Qian, G.; Lobkovsky, E. B. *Adv. Mater.* **2007**, *19*, 1693−1696.
(85) Song, X.-Z.; Song, S.-Y.; Zhao, S.-N.; Hao, Z.-M.; Zhu, M.; Meng, X.; Wu, L.-L.; Zhang, H.-J. *Adv. Funct. Mater.* **2014**, *24*, 4034−4041.
(86) Zhou, J.-M.; Shi, W.; Li, H.-M.; Li, H.; Cheng, P. *J. Phys. Chem. C* **2014**, *118*, 416−426.
(87) Hu, Z. C.; Lustig, W. P.; Zhang, J. M.; Zheng, C.; Wang, H.; Teat, S. J.; Gong, Q. H.; Rudd, N. D.; Li, J. *J. Am. Chem. Soc.* **2015**, *137*, 16209−16215.
(88) Zeng, M.-H.; Zhang, W.-X.; Sun, X.-Z.; Chen, X.-M. *Angew. Chem., Int. Ed.* **2005**, *44*, 3079−3082.
(89) Chen, P.-K.; Che, Y.-X.; Zheng, J.-M.; Batten, S. R. *Chem. Mater.* **2007**, *19*, 2162−2167.
(90) Korkmaz, S. A.; Karadağ, A.; Yerli, Y.; Soylu, M. S. *New J. Chem.* **2014**, *38*, 5402−5410.
(91) Chen, Q.; Xue, W.; Lin, J.-B.; Lin, R.-B.; Zeng, M.-H.; Chen, X.-M. *Dalton Trans.* **2012**, *41*, 4199−4266.
(92) Zou, G.-D.; He, Z.-Z.; Tian, C.-B.; Zhou, L.-J.; Feng, M.-L.; Zhang, X.-D.; Huang, X.-Y. *Cryst. Growth Des.* **2014**, *14*, 4430−4438.
(93) Si, C.-D.; Hu, D.-C.; Fan, Y.; Dong, X.-Y.; Yao, X.-Q.; Yang, Y.-X.; Liu, J.-C. *Cryst. Growth Des.* **2015**, *15*, 5781−5793.
(94) Liu, X.; Qu, X.; Zhang, S.; Ke, H.; Yang, Q.; Shi, Q.; Wei, Q.; Xie, G.; Chen, S. *Inorg. Chem.* **2015**, *54*, 11520−11525.

DOI: 10.1021/acs.cgd.6b00213
Cryst. Growth Des. XXXX, XXX, XXX−XXX